FOUNDATIONS
ADVANCES

ISSN: 2053-2733
journals.iucr.org/a

Coherent diffraction imaging: consistency of the assembled three-dimensional distribution

Miklós Tegze and Gábor Bortel

Acta Cryst. (2016). A**72**, 459–464

Acta Cryst A FOUNDATIONS ADVANCES

ISSN 2053-2733

Coherent diffraction imaging: consistency of the assembled three-dimensional distribution

Miklós Tegze* and Gábor Bortel

Institute for Solid State Physics and Optics, Wigner Research Centre for Physics, Hungarian Academy of Sciences, PO Box 49, Budapest, H-1525, Hungary. *Correspondence e-mail: tegze.miklos@wigner.mta.hu

Received 15 March 2016
Accepted 23 May 2016

Edited by J. Miao, University of California, Los Angeles, USA

Keywords: single-particle imaging; coherent diffraction imaging; X-ray free-electron lasers; XFELs; orientation.

The short pulses of X-ray free-electron lasers can produce diffraction patterns with structural information before radiation damage destroys the particle. From the recorded diffraction patterns the structure of particles or molecules can be determined on the nano- or even atomic scale. In a coherent diffraction imaging experiment thousands of diffraction patterns of identical particles are recorded and assembled into a three-dimensional distribution which is subsequently used to solve the structure of the particle. It is essential to know, but not always obvious, that the assembled three-dimensional reciprocal-space intensity distribution is really consistent with the measured diffraction patterns. This paper shows that, with the use of correlation maps and a single parameter calculated from them, the consistency of the three-dimensional distribution can be reliably validated.

1. Introduction

The main tool for determination of structures at the sub-nanometre scale is X-ray crystallography. X-ray crystallography needs crystals, but, unfortunately, not all molecules, viruses or other small but important biological objects can be easily crystallized. Therefore, it is of great importance to develop methods of structure determination without the need for crystals. Coherent diffraction imaging (CDI, Sayre *et al.*, 1998; Miao *et al.*, 1999, 2001, 2004, 2015; Neutze *et al.*, 2000; Hajdu, 2000; Huldt *et al.*, 2003; Chapman *et al.*, 2006, 2011; Loh *et al.*, 2010, 2012; Seibert *et al.*, 2011) exploits the short and intense pulses of an X-ray free-electron laser (XFEL) to record a diffraction image of a particle in the short time before radiation damage destroys the sample. The recorded image is very noisy and the orientation of the particle is unknown. Thousands of images of identical particles must be recorded and these images must be assembled into a consistent three-dimensional data set. In order to do this, the orientations of the individual particles have to be found.[1] Several methods for orienting the images have been developed, many of them for cryo-electron microscopy (cryo-EM), which has much in common with CDI. These methods either are based on the information in the intersection of the images (common-line methods, DeRosier & Klug, 1968; Hart, 1968; Crowther, 1971; van Heel, 1987; Frank, 1996; Penczek *et al.*, 1996; Fuller *et al.*, 1996; van Heel *et al.*, 2000; Shneerson *et al.*, 2008; Bortel & Tegze, 2011; Yefanov & Vartanyants, 2013; Zhou *et al.*, 2014)

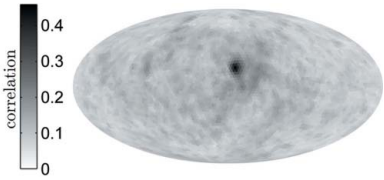

[1] In special circumstances (a very large number of very noisy images with well known noise characteristics) methods based on Bayesian information theory (Loh & Elser, 2009; Fung *et al.*, 2008; Giannakis *et al.*, 2012; Schwander *et al.*, 2012; Moths & Ourmazd, 2011; Meyer *et al.*, 2014; Walczak & Grubmüller, 2014) can produce a three-dimensional data set consistent with the measured images without finding the orientations of the individual images. These cases will be discussed later in the paper.

or use a model to start with and improve it by an iterative process (Loh & Elser, 2009; Fung *et al.*, 2008; Tegze & Bortel, 2012, 2013; Meyer *et al.*, 2014; Walczak & Grubmüller, 2014). When, finally, a three-dimensional intensity distribution is assembled, its consistency should be checked. Most iterative orientation methods can give some indications (*e.g.* a sudden jump in some parameters) that the solution is found (Tegze & Bortel, 2012), but these are not always clear. There also could be images of different particles or aggregates included in the solution which do not fit and should be left out.

Here we show a reliable method to test the consistency of the assembled three-dimensional distribution. The method is also useful to identify and reject individual images due to contamination. First we will discuss the basics of CDI experiments, and then introduce the concept of correlation maps and the consistency parameter. Finally, we discuss some special cases, when difficulties may arise.

2. Coherent diffraction imaging experiments

In CDI experiments a stream of identical particles is injected into the XFEL beam. When the short and very intense X-ray pulse hits the particle, the particle becomes highly ionized and explodes due to the strong Coulomb forces. However, this explosion needs time to develop. If the X-ray pulse is short enough (a few femtoseconds), then the X-rays scattered elastically by the particle will give information on its undamaged structure (Solem, 1986; Neutze *et al.*, 2000). The scattered X-rays are recorded by a two-dimensional detector. The measured patterns represent spherical sections of the three-dimensional intensity distribution in reciprocal space (part of the Ewald spheres). The centre of the diffraction patterns (corresponding to forward scattering) coincides with the origin of the three-dimensional reciprocal space. Many (thousands or even millions) of diffraction patterns are recorded on randomly oriented particles. These diffraction patterns are then assembled into a three-dimensional intensity distribution by an orientation algorithm (Shneerson *et al.*, 2008; Fung *et al.*, 2008; Loh & Elser, 2009; Bortel & Tegze, 2011; Tegze & Bortel, 2012, 2013; Yefanov & Vartanyants, 2013; Kassemeyer *et al.*, 2013; Zhou *et al.*, 2014; Hosseinizadeh *et al.*, 2014). If the diffraction patterns are measured up to a scattering vector $q_{\max}$, then the three-dimensional distribution will also have a radius of $q_{\max}$.

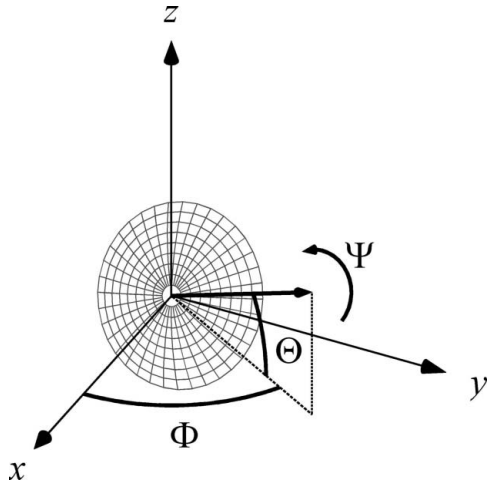

Figure 1
Orientation of an image (here represented by a grid) is defined by the Euler angles Φ, Θ and Ψ.

3. Correlation map

Here we introduce the concept of correlation maps, which can be used to test the consistency of the measured images with the three-dimensional distribution assembled by any method.

To check the consistency of the three-dimensional distribution we compare it to the measured images M_m ($m = 1 \ldots N_M$, where N_M is the number of images) in all possible orientations. Only the measured images and the assembled three-dimensional distribution are used in the comparison. The orientations of the images determined during the orientation process or even the knowledge of the method used to orient the images are not necessary. Orientation of an image can be defined by the three Euler angles Φ, Θ and Ψ (Fig. 1). The first two angles (Θ, Φ) describe the direction of a unit vector normal to the image, while the angle Ψ gives the rotation about this normal vector as an axis, *i.e.* the rotation of the two-dimensional image about its centre. We set up an approximately uniform grid (Θ_n, Φ_n) of the orientation subspace (Θ, Φ) (Tegze & Bortel, 2012). The angular distance $\delta_{\rm grid}$ between neighbouring grid points is chosen according to the pixel size Δq of the image as $\delta_{\rm grid} \leq \Delta q/k$ (k is the wavenumber of the X-rays and radius of the Ewald sphere). Here we suppose that the pixel size is chosen correctly, *i.e.* satisfying the requirements of (over)sampling (Sayre *et al.*, 1998; Miao *et al.*, 2003). We use only parts of the images inside a circle inscribed into them, corresponding to a sphere of the radius $q_{\max}$ in the three-dimensional distribution. We cut spherical sections S_n with all (Θ_n, Φ_n) orientations from the three-dimensional distribution. The choice of the Ψ angle is arbitrary at this point. Since the data in the images and in the three-dimensional distribution are usually defined on rectangular grids, we will need interpolation. We transform both the images M_m and the cut sections S_n to an evenly spaced polar grid (ϑ_i, φ_j) with $\vartheta_i = i\Delta\vartheta$, $i = 1 \ldots N_\vartheta$, $N_\vartheta \Delta\vartheta = \vartheta_{\max}$ and $\varphi_j = j\Delta\varphi$, $j = 1 \ldots N_\varphi$, $N_\varphi \Delta\varphi = 2\pi$. Note that $2k \sin(\vartheta_{\max}/2) = q_{\max}$ and the azimuthal coordinate φ and Euler angle Ψ represent rotations about the same axis.

Now we can compare each image M_m to each cut section S_n rotated by $\Psi_{j'} = j'\Delta\varphi$, $j' = 1 \ldots N_\varphi$. The similarity of two sets of data $\{a_j\}$ and $\{b_j\}$, $j = 1 \ldots N$, can be expressed in terms of the Pearson correlation (Rodgers & Nicewander, 1988):

$$C_{\rm P}\big(\{a_j\}, \{b_j\}\big) = \frac{\sum_j (a_j - \overline{a})(b_j - \overline{b})}{\left[\sum_j (a_j - \overline{a})^2\right]^{1/2} \left[\sum_j (b_j - \overline{b})^2\right]^{1/2}}$$

where $\overline{a} = (1/N)\sum_j a_j$. We compute the correlation between an image M_m and cut section S_n rotated relative to each other by $\Psi_{j'}$ about the centre as

$$c_{mnj'} = \frac{1}{N_\vartheta}\sum_{i=1}^{N_\vartheta} C_{\rm P}\big(\{M_m(\vartheta_i, \varphi_j)\}, \{S_n(\vartheta_i, \varphi_{j-j'})\}\big).$$

Here we used the equality $S_n(\vartheta_i, \varphi_j - \Psi_{j'}) = S_n(\vartheta_i, \varphi_{j-j'})$. The Pearson correlation $C_{\rm P}$ is calculated along index j for each circle of the image and these correlations are averaged. This construction has the advantage that the correlation matrix elements can be calculated for all $\Psi_{j'}$ angles at the same time with the help of fast Fourier transform (FFT) algorithms using the cross-correlation theorem (Weisstein, 2016). The correlation of a given image M_m and the cut section S_n depends on the three Euler angles: $c_{mnj'} = c_m(\Theta_n, \Phi_n, \Psi_{j'})$. In principle, this function could be used for the consistency test; however, it is not easy to comprehend. To make it more useful, we take the maxima for the relative rotation $\Psi_{j'}$:

$$c_m^{\max}(\Theta_n, \Phi_n) = \max_{j'} c_m(\Theta_n, \Phi_n, \Psi_{j'}).$$

The function $c_m^{\max}(\Theta_n, \Phi_n)$ can be plotted as a Mollweide projection in order to map the three-dimensional directions to a two-dimensional graph. The Mollweide projection (Feeman, 2000) is an equal-area map projection generally used for global maps of the world or night sky. This plot shows the best achievable agreement of the three-dimensional distribution and a given image as the function of its axis direction. If the three-dimensional distribution is correct and the image M_m corresponds to the same (asymmetric) particle, then this correlation map should feature a single, well pronounced peak above a more or less constant background.

We will show the usefulness of the correlation map using the example of the lysozyme molecule. A great number (N_M = 20 000) of synthetic CDI patterns were calculated for randomly oriented molecules using structure data from the Protein Data Bank (PDB entry 3lzt, Walsh *et al.*, 1998). The images were oriented using the correlation maximization (CM) method (Tegze & Bortel, 2012). Details of the simulation and the orientation process were described in our earlier papers (Tegze & Bortel, 2012, 2013). The CM method starts initially from a random three-dimensional distribution and constructs the next three-dimensional distribution from all images in the best-fitting orientations. Fig. 2 shows the correlation maps of a randomly selected image at the beginning (*a*), just before (*b*) and after (*c*) convergence is reached. The map at the beginning of the orientation process is rather featureless (Fig. 2*a*). Just before convergence, the correlation map shows some broad features (Fig. 2*b*) but they are very different from the single narrow peak appearing when convergence is reached (Fig. 2*c*). The maximum correlation of the peak depends basically on the noisiness of the image, since the three-dimensional distribution assembled from many images has much less noise. For noiseless images the correlation maximum should be slightly below unity (allowing for small errors due to the interpolations).

If the particle has rotational symmetry, then a measured diffraction image may fit in more than one orientation to the three-dimensional distribution and more than one peak may appear on the map. The number of peaks depends on the symmetry and can be reduced in some special orientations of the particle. The treatment of symmetry in the orientation process and in the correlation map goes beyond the scope of the present work and we will discuss it in a forthcoming paper. We note here only that in the case of symmetric particles the correlation map for a consistent three-dimensional distribution would show peaks of about equal heights.

In the asymmetric case, the presence of the single narrow peak in all correlation maps for each image indicates that we have a consistent three-dimensional distribution and all images correspond to the same type of particle. If not all but many correlation maps show the distinct peak, then we still have a consistent three-dimensional distribution and the correlation maps with peaks correspond to identical particles. The maps without the peak belong to other kinds of particles (different conformations, contaminants, solvent droplets *etc.*) and their contribution should be left out from the three-dimensional distribution (Tegze & Bortel, 2013). In Fig. 3 we show correlation maps calculated for images of lysozyme, cytochrome (PDB entry 2xl6, Hough *et al.*, 2011) and Arg–lysozyme (a complex of lysozyme with arginine, PDB entry 3agi, Ito *et al.*, 2011) molecules and a three-dimensional distribution assembled from lysozyme images only.

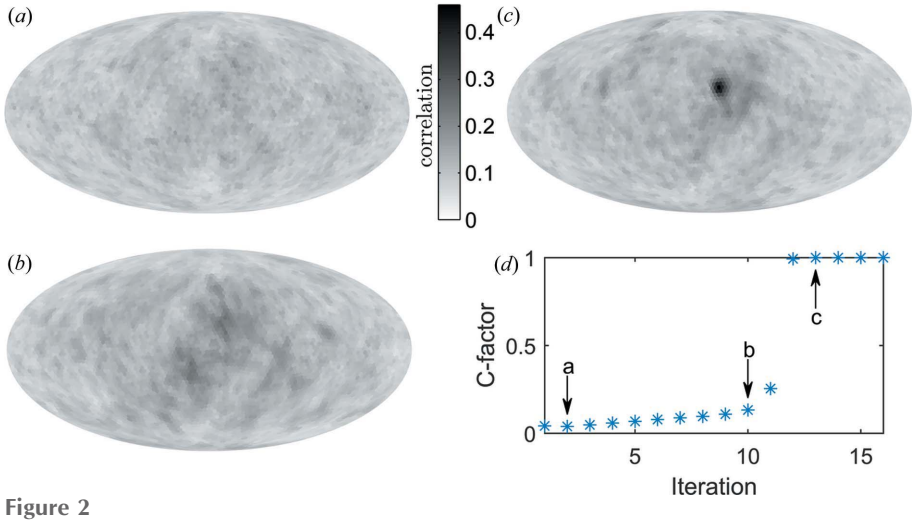

Figure 2
Correlation maps and *C* factor. Correlation maps of a randomly selected diffraction image of lysozyme at various stages of the iteration process by the CM method (*a*)–(*c*). *C* factor as a function of iteration number (*d*). The arrows indicate the values corresponding to the correlation maps shown on (*a*)–(*c*).

4. *C* factor

In the previous section we have shown that looking at the correlation maps can help us to decide whether the assembled three-dimensional distribution is consistent or not. However, when a great number of images are used to construct the three-dimensional distri-

bution, it is not easy to check all correlation maps visually. So we need a single parameter indicating the measure of confidence in our assembled three-dimensional distribution. This confidence parameter should be near to unity if all correlation maps feature single peaks well above the background and near to zero otherwise. Here we describe how such a parameter can be calculated from the correlation maps.

First we find the angles $(\Theta_{n_m^{\max}}, \Phi_{n_m^{\max}})$ corresponding to the maxima of the $c_m^{\max}(\Theta_n, \Phi_n)$ correlation maps. Then we exclude a circular region around the maximum. The radius of the region should be larger than the expected width of the peak so that this region would contain the peak if it exists. A safe estimate for the radius of the excluded angular region is 0.25 rad. Now we can calculate the mean $\overline{c_m^{\rm bg}}$ and standard deviation $\sigma_m^{\rm bg}$ of the background for each correlation map and take their average $\overline{c_{\rm bg}}$ and $\overline{\sigma_{\rm bg}}$, respectively. If

$$c_m^{\max}(\Theta_{n_m^{\max}}, \Phi_{n_m^{\max}}) > \overline{c_{\rm bg}} + 6\overline{\sigma_{\rm bg}}$$

then we can be confident that the peak rises well out of the background and the corresponding image fits well to the three-dimensional distribution in one orientation. Let us call the number of images satisfying the above condition $N_{\rm peak}$. We define the confidence parameter (C factor, in analogy with the crystallographic R factor) as the fraction of well fitting images:

$$C = N_{\rm peak}/N_M.$$

The value of the C factor is one if all images fit well in one orientation and close to zero if only a few or none fit well. We show the development of the C factor during orientation of simulated lysozyme diffraction images in Fig. 2(*d*).

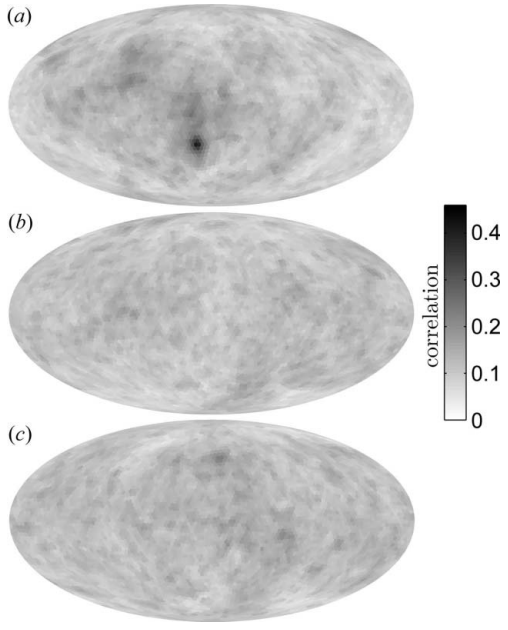

Figure 3
Correlation maps of lysozyme (*a*), cytochrome (*b*) and Arg–lysozyme (*c*) diffraction images with a consistent three-dimensional distribution assembled from lysozyme images. The map for lysozyme shows a strong peak, while the one for cytochrome shows none. Since Arg–lysozyme consists of a slightly distorted lysozyme and a much smaller arginine, a very weak peak appears on the corresponding map.

We tested the confidence parameter for simulated diffraction images of various molecules and various levels of noise. In most of the cases the C factor indicates well that the images are correctly oriented ($C \simeq 1$). There were two notable exceptions: when images of different molecules were mixed and when relatively few (a few hundreds instead of many thousands) images were used to construct the three-dimensional distribution.

If the value of the C factor is below one, this may indicate that images of more than one kind of particle are mixed. Then one should select those images that satisfy the condition above and try to assemble a three-dimensional distribution from them (Tegze & Bortel, 2013).

When relatively few images are used for assembling the three-dimensional distribution, the confidence parameter is not reliable. In the top panel of Fig. 4 we plotted the C factor as a function of the number of images for the three-dimensional distributions assembled from the correctly oriented images (circles) and from the same images oriented randomly (triangles). It is clear that the C factor cannot distinguish between these two cases if the number of images is below a few hundred. The reason for this is very simple. When assembling the three-dimensional distribution from a small number of images, only a couple of images contribute to each

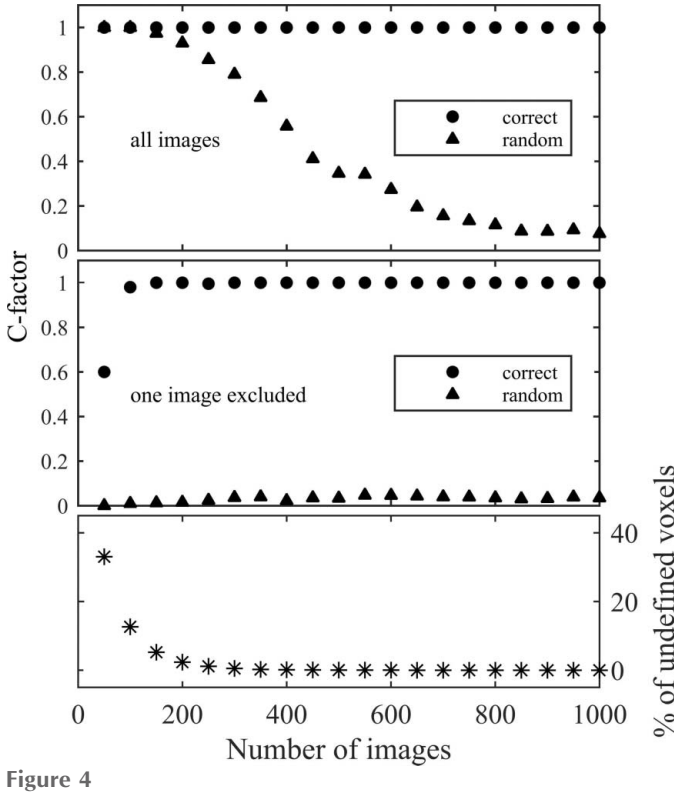

Figure 4
Dependence of the C factor on the number of images. Circles and triangles indicate values for three-dimensional distributions assembled from correctly and randomly oriented images, respectively. Top panel: the three-dimensional distribution is assembled from all images. Middle panel: the image, for which the correlation map is calculated, is excluded from the three-dimensional distribution. Bottom panel: asterisks indicate the percentage of undefined voxels in the three-dimensional distribution assembled from all correctly oriented images.

voxel, except in a small region in the centre. If an image is compared to the three-dimensional distribution in the same orientation in which the image was used for assembling the three-dimensional distribution, the correlation will always be high, independent of how the image was oriented. To avoid this problem, when making the correlation map for a certain image, we should compare the image to a three-dimensional distribution assembled from all images but excluding that single image. This means that we have to construct as many three-dimensional distributions as the number of images. Fortunately, we have to do this only when the number of images is not very large. Technically, we can construct the distribution from all images and then subtract the contributions of the single image in question. The *C* factor derived from correlation maps calculated by the above method is reliable also for a relatively small number of images (middle panel of Fig. 4). It becomes unreliable only when the number of images is so small that many voxels of the three-dimensional distribution are undefined (bottom panel of Fig. 4).

5. Applicability and limitations

The correlation maps and the *C* factor give reliable information on the consistency of the assembled three-dimensional distribution produced by any method, if the noise level of the images allows the determination of their orientations. However, in cases when the signal-to-noise ratio in the measured images is very low, orientations of the individual images cannot be found. If the statistical properties of the noise are well known and a very large number of images are measured, then methods based on Bayesian information theory (Loh & Elser, 2009; Fung *et al.*, 2008; Giannakis *et al.*, 2012; Schwander *et al.*, 2012; Moths & Ourmazd, 2011; Meyer *et al.*, 2014, Walczak & Grubmüller, 2014) can produce a three-dimensional data set consistent with the measured images without finding the orientations of the individual images. In practice, other, not very well characterized contributions (originating *e.g.* from the electronic noise and imperfections of the detector) to the noise are always present, which may prohibit the success of these methods for images with such very low signal-to-noise ratio. If the same methods are applied to images with lower noise level, then the orientations of the individual images can be found, and the correlation maps and the *C* factor can be used reliably to test the consistency of the three-dimensional distribution.

In our view such validation should be performed on all three-dimensional intensity distributions assembled by any method from CDI experimental data before attempting the real-space density reconstruction. This would characterize the quality of the diffraction data separately from the reconstructed structure, and could prevent unreliable or possibly false results from being obtained.

Finally, we note that the correlation maps and the *C* factor introduced in this paper could also be used in the case of cryo-EM.

6. Summary

We have introduced the concept of correlation maps and the *C* factor (confidence parameter) to test the consistency of three-dimensional distributions assembled from images of single-particle experiments. We have shown that for all practical cases, when the particle has no symmetry, the appearance of a single peak in all correlation maps or the value of the *C* factor indicate that the three-dimensional distribution is consistent with the measured images. This validation method works well for three-dimensional distributions assembled by any (iterative or common-line) methods. We proposed the use of the *C* factor for verification of all three-dimensional assembled diffraction data. The method in its present form is not applicable to particles with symmetry. The case of symmetric particles will be discussed in a forthcoming paper. The results presented here, with some modifications, could be applied for the case of cryo-electron microscopy as well.

Acknowledgements

We are grateful to G. Oszlányi for discussions. This work was supported by the Hungarian OTKA grants K81348, NK105691 and K115504 of the National Research Development and Innovation Office – NKFIH.

References

Bortel, G. & Tegze, M. (2011). *Acta Cryst.* A**67**, 533–543.
Chapman, H. N. *et al.* (2006). *Nat. Phys.* **2**, 839–843.
Chapman, H. N. *et al.* (2011). *Nature (London)*, **470**, 73–77.
Crowther, R. A. (1971). *Philos. Trans. R. Soc. London Ser. B*, **261**, 221–230.
De Rosier, D. J. & Klug, A. (1968). *Nature (London)*, **217**, 130–134.
Feeman, T. G. (2000). *SIAM Rev.* **42**, 109–114.
Frank, J. (1996). *Three-dimensional Electron Microscopy of Macromolecular Assemblies.* San Diego: Academic Press.
Fuller, S. D., Butcher, S. J., Cheng, R. H. & Baker, T. S. (1996). *J. Struct. Biol.* **116**, 48–55.
Fung, R., Shneerson, V., Saldin, D. K. & Ourmazd, A. (2008). *Nat. Phys.* **5**, 64–67.
Giannakis, D., Schwander, P. & Ourmazd, A. (2012). *Opt. Express*, **20**, 12799–12826.
Hajdu, J. (2000). *Curr. Opin. Struct. Biol.* **10**, 569–573.
Hart, R. G. (1968). *Science*, **159**, 1464–1467.
Heel, M. van (1987). *Ultramicroscopy*, **21**, 111–124.
Heel, M. van, Gowen, B., Matadeen, R., Orlova, E. V., Finn, R., Pape, T., Cohen, D., Stark, H., Schmidt, R., Schatz, M. & Patwardhan, A. (2000). *Q. Rev. Biophys.* **33**, 307–369.
Hosseinizadeh, A., Schwander, P., Dashti, A., Fung, R., D'Souza, R. M. & Ourmazd, A. (2014). *Philos. Trans. R. Soc. London Ser. B*, **369**, 20130326.
Hough, M. A., Antonyuk, S. V., Barbieri, S., Rustage, N., Mckay, A. L., Servid, A. E., Eady, R. R., Andrew, C. R. & Hasnain, S. S. (2011). *J. Mol. Biol.* **405**, 395–409.
Huldt, G., Szőke, A. & Hajdu, J. (2003). *J. Struct. Biol.* **144**, 219–227.
Ito, L., Shiraki, K., Matsuura, T., Okumura, M., Hasegawa, K., Baba, S., Yamaguchi, H. & Kumasaka, T. (2011). *Protein Eng. Des. Sel.* **24**, 269–274.
Kassemeyer, S., Jafarpour, A., Lomb, L., Steinbrener, J., Martin, A. V. & Schlichting, I. (2013). *Phys. Rev. E*, **88**, 042710.
Loh, N. D. *et al.* (2010). *Phys. Rev. Lett.* **104**, 225501.

Loh, N. D. & Elser, V. (2009). *Phys. Rev. E*, **80**, 026705.
Loh, N. D. *et al.* (2012). *Nature (London)*, **486**, 513–517.
Meyer, J. C., Kotakoski, J. & Mangler, C. (2014). *Ultramicroscopy*, **145**, 13–21.
Miao, J., Chapman, H. N., Kirz, J., Sayre, D. & Hodgson, K. O. (2004). *Annu. Rev. Biophys. Biomol. Struct.* **33**, 157–176.
Miao, J., Charalambous, P., Kirz, J. & Sayre, D. (1999). *Nature (London)*, **400**, 342–344.
Miao, J., Hodgson, K. O. & Sayre, D. (2001). *Proc. Natl Acad. Sci. USA*, **98**, 6641–6645.
Miao, J., Ishikawa, T., Anderson, E. H. & Hodgson, K. O. (2003). *Phys. Rev. B*, **67**, 174104.
Miao, J., Ishikawa, T., Robinson, I. K. & Murnane, M. M. (2015). *Science*, **348**, 530–535.
Moths, B. & Ourmazd, A. (2011). *Acta Cryst.* A**67**, 481–486.
Neutze, R., Wouts, R., van der Spoel, D., Weckert, E. & Hajdu, J. (2000). *Nature (London)*, **406**, 752–757.
Penczek, P. A., Zhu, J. & Frank, J. (1996). *Ultramicroscopy*, **63**, 205–218.
Rodgers, J. L. & Nicewander, W. A. (1988). *Am. Stat.* **42**, 59–66.
Sayre, D., Chapman, H. N. & Miao, J. (1998). *Acta Cryst.* A**54**, 232–239.
Schwander, P., Giannakis, D., Yoon, C. H. & Ourmazd, A. (2012). *Opt. Express*, **20**, 12827–12849.
Seibert, M. M. *et al.* (2011). *Nature (London)*, **470**, 78–81.
Shneerson, V. L., Ourmazd, A. & Saldin, D. K. (2008). *Acta Cryst.* A**64**, 303–315.
Solem, J. C. (1986). *J. Opt. Soc. Am. B*, **3**, 1551–1565.
Tegze, M. & Bortel, G. (2012). *J. Struct. Biol.* **179**, 41–45.
Tegze, M. & Bortel, G. (2013). *J. Struct. Biol.* **183**, 389–393.
Walczak, M. & Grubmüller, H. (2014). *Phys. Rev. E*, **90**, 022714.
Walsh, M. A., Schneider, T. R., Sieker, L. C., Dauter, Z., Lamzin, V. S. & Wilson, K. S. (1998). *Acta Cryst.* D**54**, 522–546.
Weisstein, E. W. (2016). Cross-correlation theorem. From *MathWorld – a Wolfram web resource.* http://mathworld.wolfram.com/Cross-CorrelationTheorem.html.
Yefanov, O. M. & Vartanyants, I. A. (2013). *J. Phys. B At. Mol. Opt. Phys.* **46**, 164013.
Zhou, L., Zhang, T.-Y., Liu, Z.-C., Liu, P. & Dong, Y.-H. (2014). *Acta Cryst.* A**70**, 364–372.